Digest Journal of Nanomaterials and Biostructures Vol. 5, No 4, October-December 2010, p. 981 - 988

EFFECT OF ANNEALING TEMPERATURE ON THE STRUCTURAL AND OPTICAL PROPERTIES OF ZINC OXIDE (ZnO) NANOCRYSTALS PREPARED BY SOL GEL

F.I. EZEMA*, U. O. A. NWANKWO
Department of Physics & Astronomy,
University of Nigeria, Nsukka, Enugu State, Nigeria

In this study, Zinc Oxide crystals were grown using a combination of the gel method and thermal evaporation. The solution for the gel was maintained at a temperature of 104^{o}C, and was prepared using absolute ethanol. Identification of the chemical species of the crystals grown was done using Fourier Transform Infrared Spectroscopy (FTIR), the structural analysis was done using X-Ray Diffraction technique and optical properties were studied using UV-VIS technique. The optical band gap values were found to increase from 2.75 eV in as grown to 2.85 eV for annealed at 100^{o}C for 10minutes. This value is further increased to 2.88 eV after annealing at 150^{o}C for 10 minutes and finally to 3.00 eV when annealed at 200^{o}C. The effect of annealing temperature on the structural properties was studied using the (002) direction of the zinc oxide crystal as a focal point and showed that crystallite sizes decrease from 18.4nm to 15.3nm with increase in annealing temperature.

(Received October 5, 2010; accepted October 28, 2010)

Keywords: ZnO Nanocrystal, Sol Gel process, FTIR, XRD, Optical studies

1. Introduction

Technological advancement in recent years has led to the development of crystalline materials with certain desired qualities enabling their applications in areas like electronics (optoelectronics), spintronics, medicine, superconductivity, nuclear and electron resonance, molecular structure investigation, photonics, and photovoltaics. Some of these crystalline materials are specifically used in the manufacture of diodes, rectifiers, photovoltaic (PV) cells, scintillators, gauss metres, and particle Counters. Amongst these crystalline materials, the semi-conducting ones are of great interest because their properties can be easily modified or enhanced through doping, thus enabling them have a wide range of possible applications.

Recent developments in the semi-conductor industry have seen an increased interest in zinc oxide (ZnO) and zinc oxide based semi-conducting crystalline materials because of their current and potential applications. Currently, zinc oxide and zinc oxide based semi-conducting materials are applied in solar cells and liquid crystal displays (as front contact), rubber manufacturing, concrete manufacturing, medicine, food industry (as additive), cigarette manufacturing, and anticorrosive coatings. They also have potential applications which include applications in laser diodes and light emitting diodes, transparent thin-film transistors (TTFT), optoelectronics, spintronics, and hydrogen sensors.

Zinc Oxide is a wide-band gap group II–VI semiconductor and is typically an n-type semiconductor. In particular, it is considered a promising candidate for use as visible and ultraviolet (UV) light emitters [1]. It exhibits tuneable effect [2] and dopant-related luminescence properties in the visible region of the electromagnetic spectrum. In contrast to gallium nitride

*Corresponding author: fiezema@yahoo.com, fabian.ezema@unn.edu.ng, ufonduo@yahoo.com

(GaN), its main competitor for ultraviolet (UV) applications, ZnO exhibits favourable properties such as a high exciton binding energy of 60 meV (prospect of low laser threshold at room temperature, in contrast to 25 meV for GaN), unproblematic wet-chemical etching, radiation hardness (space applications) and the availability of substrates for homoepitaxy [1]. Zinc oxide is strongly piezoelectric with a coupling factor greater than four times that of quartz [3]. Also, it has a very low dielectric constant making it suitable for such devices as transducers [3]. Crystals of zinc oxide are also useful in acoustical amplifiers, delay lines and other electrical devices.

As a result of its huge prospects in the semiconductor industry, zinc oxide have been synthesized via pulsed laser deposition (PLD) [4], chemical vapour transport [5-8], flux method [9, 10] and hydrothermal method [11, 12].

Our aim of this study is to investigate into the effect increase in the annealing temperature of bulk ZnO crystals (grown via the gel route), will have on its structural and optical properties.

2. Experimental details

In the synthesis of zinc oxide crystals, absolute ethanol was used as solvent. Zinc acetate dihydrate [$Zn(CH_3COO)_2{\cdot}2H_2O$] was used as a source of both zinc and oxygen. Zinc acetate dihydrate was used as source of both zinc and oxygen because it is known to be a 'mono-precursor' [13]. This is a unique property of the zinc acetate dihydrate compound. Being a 'mono-precursor' means that one does not need an oxygen precursor to grow ZnO since zinc acetate dihydrate decomposes to yield zinc oxide. Decomposition of zinc acetate dihydrate to yield zinc oxide proceeds as shown below [13]:

$$4Zn(CH_3COO)_2 \text{ (solid)} \rightarrow Zn_4O(CH_3COO)_6 \text{ (solid)} + (CH_3CO)_2O \text{ (gas)}$$
$$\rightarrow Zn_4O(CH_3COO)_6 \text{ (liquid)}$$
$$\rightarrow 4ZnO \text{ (solid)} + 3CH_3COCH_3 \text{ (gas)} + 3CO_2 \text{ (gas)}$$

It therefore follows that in the use of ethanol as solvent; ethanol could be viewed as being a medium through which heat is supplied for the decomposition of zinc acetate dihydrate. The choice of ethanol as solvent was based on a recent study, in which absolute ethanol and zinc acetate dehydrate were used as precursors in the synthesis of ZnO thin films via the Sol-Gel route [14]. There are also a number of other studies where various organic compounds (e.g. Monoethanolamine, Diethanolamine, 2-Methoxy Ethanol, etc) were used as solvent for dissolving zinc acetate dihydrate [15, 16]. This shows that zinc acetate dihydrate is soluble in organic solvents.

To synthesize the zinc oxide crystals, 10g of Zinc acetate dihydrate [$Zn(CH_3COO)_2{\cdot}2H_2O$] was mixed with 25ml of absolute ethanol (C_2H_5OH) in a beaker. The resulting mixture was stirred using a magnetic stirrer for about 10 minutes after which it was placed in an oven maintained at 104^oC. The gel medium allowed for the growth of the crystals in a homogenous manner. No seed crystal or impurity was introduced into the gel mediums and as such, homogenous nucleation was the prevalent nucleation process during the nucleation phase of the growth process.

After about 120 minutes in the oven, zinc acetate dihydrate decomposed to yield ZnO. Keeping the beaker in the oven (at 104^oC) for an additional 90 minutes ensured that the solvent and any moisture present were evaporated completely, leaving behind the zinc oxide (ZnO) crystals. The crystals were then ground into finer particles using a mortar and pestle.

3. Results and discussion

3.1 FTIR Analysis

FTIR is a technique used to obtain information about the chemical bonding in a material. It is used to identify the elemental constituents of a material sample. FTIR analysis was performed using SHIMADZU FTIR. For our study, the Double-Pass Transmission mode was used. Here, the

infrared (IR) beam makes a double pass through the sample before reaching the detector. The double-pass mode was used because it offers the highest level of sensitivity [17].

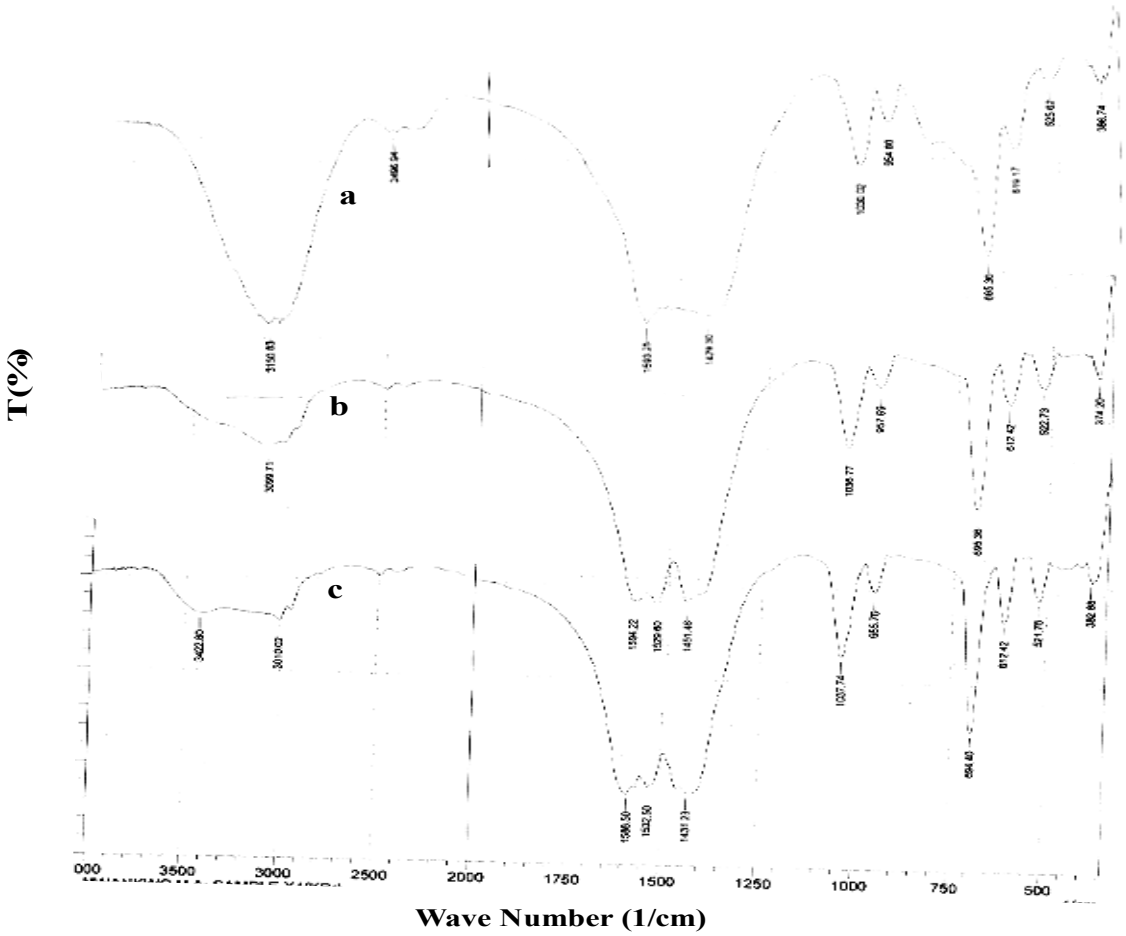

Fig. 1. FTIR Spectra of ZnO crystals – (a) As-grown, (b) Annealed for 10mins at 150^{o}C, (c) Annealed for 10mins at 200^{o}C.

Fig. 1 shows the FTIR spectra of ZnO crystal annealed at various temperatures for 10 minutes. In Fig. 1(a), we observe various peaks as indicated, showing the main absorption bands. These absorption bands are due to O-H bending of the hydroxyl group at 1429.3cm^{-1} [18] and O-H out-of-plane bending of the hydroxyl group at 619.17cm^{-1} and 695.26cm^{-1} [18]; Zn-O stretching of ZnO at 386.74cm^{-1} [19]; and an O-H stretching of hydroxyl group at 3150.83cm^{-1} [18, 20]. Fig. 1(b) show absorption bands due to O-H bending of the hydroxyl group at 1451.48cm^{-1} [18] and O-H out-of-plane bending of the hydroxyl group at 612.42cm^{-1} and 695.36cm^{-1} [18]; Zn-O stretching of ZnO at 374.2cm^{-1} [19]; and an O-H stretching of hydroxyl group at 3099.71cm^{-1} [18, 20]. Similarly, Fig. 1(c) show absorption bands due to O-H bending of the hydroxyl group at 1431.23cm^{-1} [18] and O-H out-of-plane bending of the hydroxyl group at 612.42cm^{-1} and 694.4cm^{-1} [18]; Zn-O stretching of ZnO at 382.88cm^{-1} [19]; and an O-H stretching of hydroxyl group at 3422.80cm^{-1} [18, 20].

The presence of the absorption peak associated with the Zn-O bond in each spectra show clearly the presence of zinc oxide crystals in the samples. This confirms that the crystal sample analysed is composed of zinc oxide crystals. From the spectra shown in Fig. 1(a-c), we observe a splitting of the IR peak corresponding to O-H bending of the hydroxyl group (1410-1310cm^{-1}) and that corresponding to O-H stretching of the hydroxyl group (3500-3000cm^{-1}). This splitting could be attributed to the dissociation of the OH molecule due to increase in annealing temperature.

3.2 Structural Analysis

XRD was used to uniquely identify the crystalline phases present in the crystals and to measure the structural properties. The XRD characterisation of crystal samples were carried out using MD-10 Diffractometer. The diffractometer recorded diffractograms using CuK_{α} radiation. Diffraction patterns of the samples were recorded in the 2θ range from 10^{o} to 72^{o}.

The XRD spectra in the figures below show that the compounds grown are crystalline in nature. For each of these XRD spectra, the crystallite size D, was determined using the Debye Scherrer formula [19, 21-23] as given below:

$$D = \frac{K\lambda}{\beta \cos \theta} \tag{1}$$

where K = 0.9, is the shape factor, λ = 1.5408Å, θ is the diffraction peak angle (Bragg Angle) in degrees, and β denotes the full width at half maximum (FWHM) in radians, of the corresponding diffraction peak.

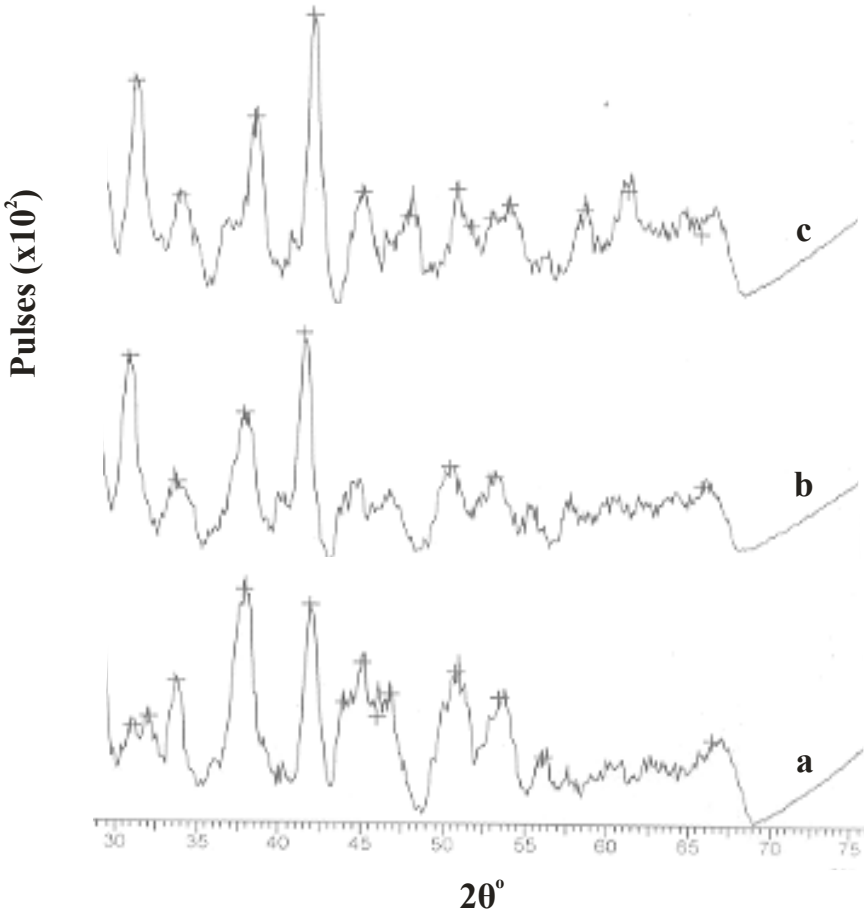

Fig. 2. XRD Spectrum for ZnO crystals – 'a' = As grown, 'b' = Annealed at 150°C for 10 minutes, 'c' = Annealed at 200°C for 10 minutes.

Fig. 2 above shows the XRD spectra of ZnO. The spectrum in Fig. 2(a), shows that the crystal is crystallized in the wurtzite phase (i.e. has the Zinc Blende wurtzite structure). This spectrum has peaks which are related to hexagonal phase ZnO. The peaks and their corresponding planes are as follows: (100) for $2\theta^{o} = 32.02$, (002) for $2\theta^{o} = 33.68$, (102) for $2\theta^{o} = 46.72$, (110) for $2\theta^{o} = 56.10$ and (200) for $2\theta^{o} = 66.41$. These are comparable to the most frequently observed XRD peaks in many related studies [23-31]. The (100) peak is labelled as a-axis related and the (002) as

the c-axis related [5]. The presence of various peaks corresponding to planes other than the (002) plane shows that sample is polycrystalline in nature [26]. Using the Debye Sherrer formula the crystallite size of the (002) plane [24] was found to be 18.4nm.

For ZnO crystals annealed for 10 minutes at 105^{o}C, its spectrum (Fig. 2(b)) also shows that the crystal has the Zinc Blende wurtzite structure with corresponding spectral peaks. These peaks and their corresponding planes are as follows: (100) for $2\theta^{o}$ = 31.28, (002) for $2\theta^{o}$ = 34.25 and (200) for $2\theta^{o}$ = 66.20. These peaks are comparable to that reported in various studies [23-31]. Here, the crystallite size of the (002) plane [24] was found to be 16.2nm. Similarly, the spectrum of ZnO crystals annealed for 10 minutes at 200^{o}C (Fig. 2(c)) also shows that the crystal has the Zinc Blende wurtzite structure with corresponding spectral peaks. The peaks and their corresponding planes are as follows: (100) for $2\theta^{o}$ = 31.70, (002) for $2\theta^{o}$ = 34.39 and (200) for $2\theta^{o}$ = 66.01; and are comparable to that reported in various studies [23-31]. Here, the crystallite size of the (002) plane [24] was found to be 15.3nm.

From the foregoing discussion of the XRD results, we observe that an increase in the annealing temperature of Zinc Oxide crystals introduces variations in its structural properties. This variation is shown in table 1, for the (002) plane crystallite size and full width at half maximum (FWHM).

Table 1. Variation of the (002) Plane Crystallite Size and Full Width at Half Maximum (FWHM) of ZnO Crystals with Annealing Temperature.

Sample	Annealing Temperature (^{o}C)	Crystallite Size (nm)	FWHM (radians)
a	As-grown	18.4	1.1002
b	150	16.2	1.0346
c	200	15.3	0.9055

3.3 Optical Studies

Optical absorption studies of the crystalline particle colloids were carried out using a JENWAY 6405 UV-VIS spectrophotometer operating at a wavelength range of 200nm to 1200nm at intervals of 5nm. In the optical absorption study, deionised water was used as reference solution [32]. First, the crystal samples were dissolved in deionised water forming a colloidal solution which is then subjected to UV-VIS analysis.

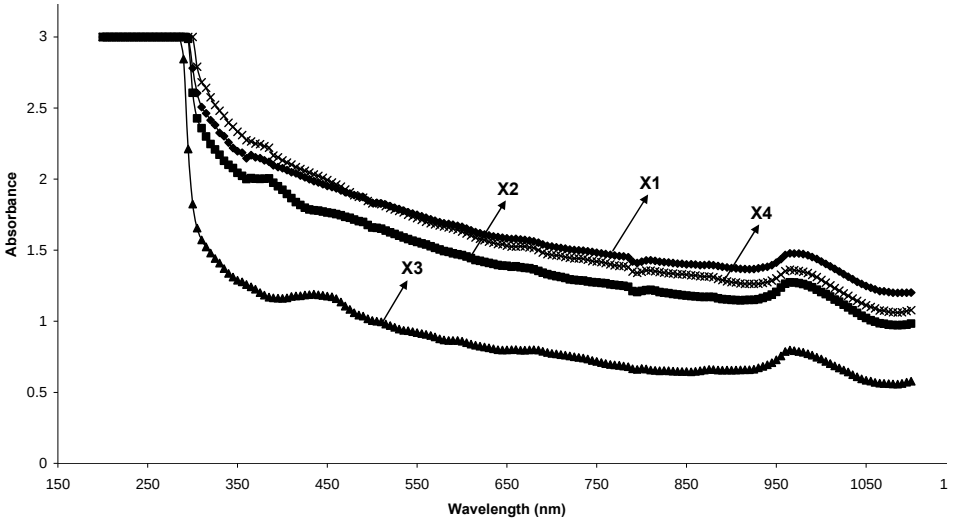

Fig. 3. Optical absorption spectra of ZnO crystals – (X1 = As-grown, X2 = Annealed for 10mins at 100^{o}C, X3 = Annealed for 10mins at 150^{o}C, X4 = Annealed for 10mins at 200^{o}C)

The optical absorption spectra above show that annealing ZnO crystals at temperatures up to 150^{o}C decreases its absorbance steadily. The sample annealed at 200^{o}C (X4) showed a deviation as it has a higher absorbance compared with others (X2 and X3), though its absorbance is still lower than the as-grown sample (X1). The absorption spectrum shows that ZnO crystals have a low absorbance in the visible region, which is a characteristic of ZnO.

Fig. 4 shows the direct band gap plots. From the figure, X1 (as-grown) has a band gap of 2.75eV, X2 (annealed for 10mins at 100^{o}C) has a band gap of 2.85eV, X3 (annealed for 10mins at 150^{o}C) has a band gap of 2.88eV, while X4 (annealed for 10mins at 100^{o}C) has a band gap of 3.0eV. This shows that an increase in the annealing temperature increases the band gap. The increase in band gap could be attributed to the evaporation of impurity ions (OH^- ions) which causes a lowering of the band gap.

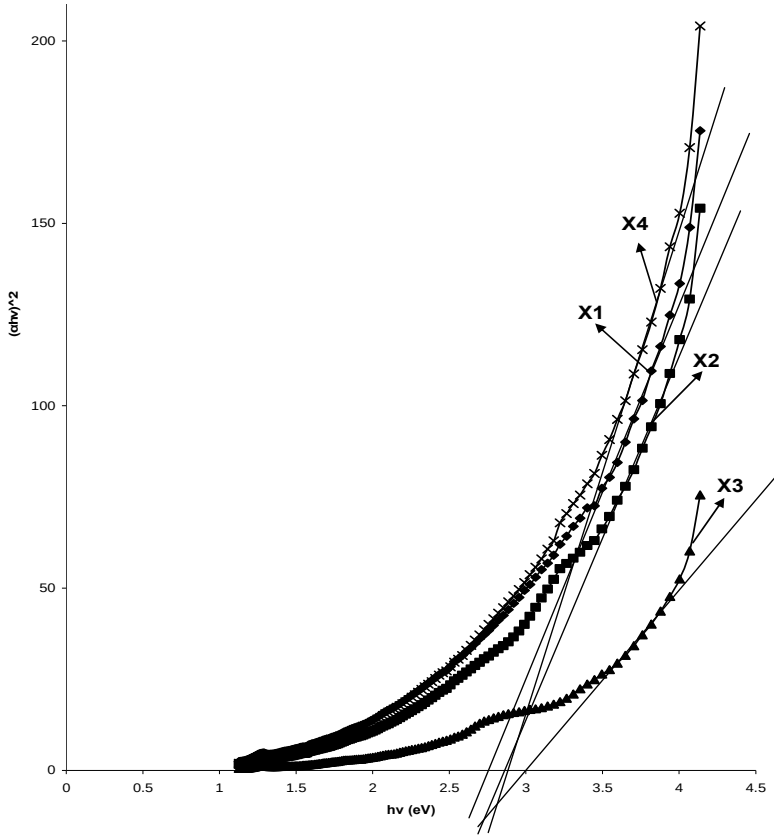

Fig. 4. Plot of Band Gap (Direct) for different annealing temperatures.

The Urbach's energy, which corresponds to the width of the tail of localised states within the optical band gap, it is linked to the absorption coefficient in the lower energy region of fundamental edge and is shown in figure 5. Urbach's energy can be deduced from the absorption coefficient (α) and depends on structural defects [33]. It is determined by plotting ln(α) against photon energy [34] , and extrapolating to the photon energy axis. Ubarch's energy determined for as-grown ZnO crystals (X1) is 0.7eV, for ZnO crystals annealed at 100^{o}C for 10mins is 0.88eV, for ZnO crystals annealed at 150^{o}C for 10mins is 1.15eV, while that for ZnO crystals annealed at 200^{o}C for 10mins is 0.80eV. We observe that the Urbach's energy increases with an increase in annealing temperature. Sample X4 showed a drop in the Urbach's energy as compared to sample X3. This might be due to the breakdown of crystalline structure of ZnO at high annealing temperature.

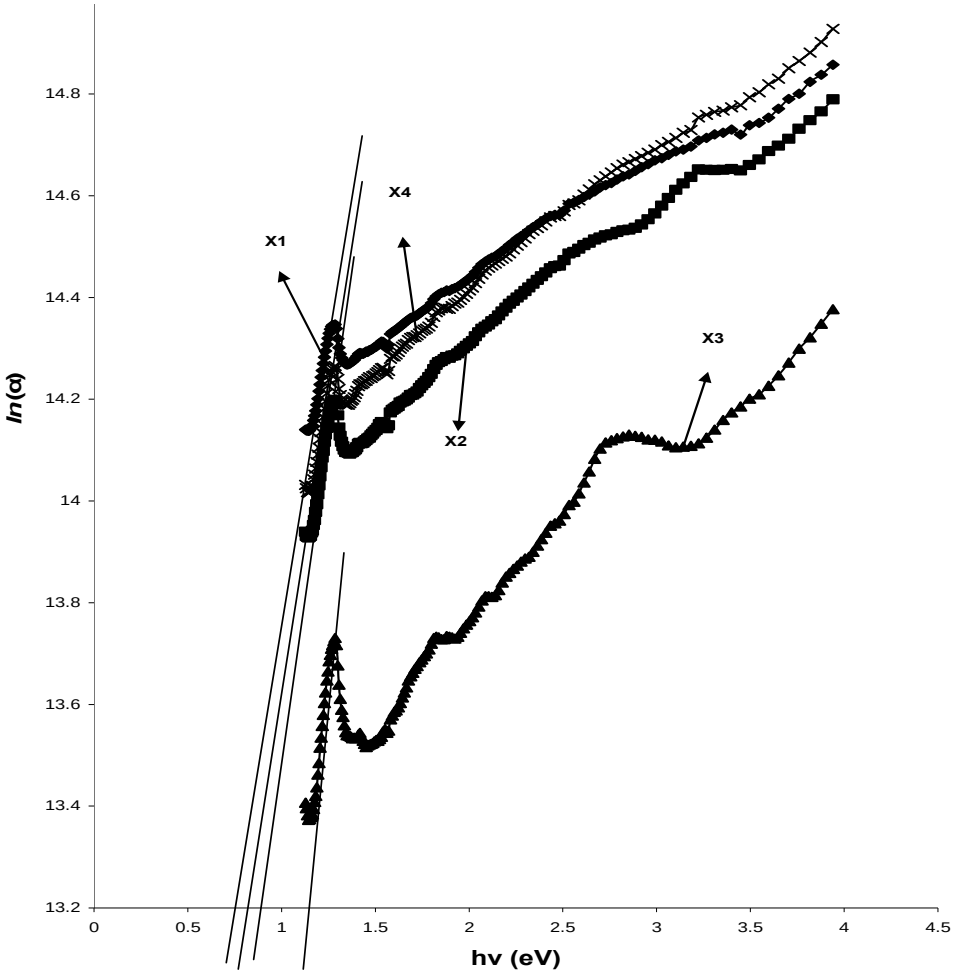

Fig. 5. Urbach's Energy Plot

4. Conclusion

Annealing zinc oxide crystals at higher temperatures, results in higher quality crystals. We observe that an increase in the annealing temperature results in a decrease in the crystallite size of the (002) plane. This is evident from the crystallite sizes calculated. Also we observe that for zinc oxide crystals, increase in annealing temperature results in a decrease in the width of the diffraction peak of the (002) plane. This shows that annealing at higher temperatures produces pure zinc oxide crystals. Optical studies show that subjecting ZnO crystals to increasing annealing temperature decreases its absorbance, while increasing its band gap (direct), as well as increasing the Urbach's energy.

References

[1] M. Grundmann, A. Rahm, T. Nobis, M. Lorenz, C. Czekalla, M.K. Evgeni, J. Lenzner, N. Boukos, A. Travlos, Growth and Characterization of ZnO Nano- and Microstructures in Handbook of Self Assembled Semiconductor Nanostructures for Novel Devices in Photonics and Electronics. Mohamed Henini (Ed.), Elsevier Ltd. 293-295 (2008).
[2] H. Y. Yang, S.F. Yu, S.P. Lau, J. Crystal Growth. **312**, 16–18 (2009).
[3] J.W. Berry, A.J. Deutschman, United States Patent 3615264. Published 10/26/1971.
[4] J.H. Choi, H. Tabata, T. Kawai, J. Crystal Growth. **226,** 493 (2001).
[5] S. Jung, W. Cho, H.J. Lee, M. Oh, Angew. Chem. Int. Ed. **48**, 1459 (2009).
[6] D.C. Look, D.C. Reynolds, J.R. Sizelove, R.L. Jones, C.W. Litton, G. Cantwell, W.C. Harsch, Solid State Commun. **105,** 399 (1998).

[7] K. Matsumoto, K. Noda, J. Crystal Growth. **102**, 137 (1990).
[8] J.-M. Ntep, S.S. Hassani, A. Lusson, A. Tromson-Carli, D. Ballutaud, G. Didier, R. Triboulet, J. Crystal Growth. 207, 30 (1999).
[9] K. Oka, H. Shibata, S. Kashiwaya, J. Crystal Growth **237–239**, 5 (2002)
[10] N. Ohashi, T. Sekiguchi, K. Aoyama, T. Ohgaki, Y. Terada, I. Sakaguchi, T. Tsurumi, H. Haneda, J. Appl. Phys. **91**, 3658 (2002).
[11] T. Sekiguchi, S. Miyashita, K. Obara, T. Shishido, N. Sakagami, J. Crystal Growth. **214/215**, 72 (2000).
[12] T. Sakagami, M. Yamashita, T. Sekiguchi, S. Miyashita, K. Obara, T. Shishido, J. Crystal Growth. **229**, 98 (2001).
[13] A. Wójcik, M. Godlewski1, E. Guziewicz, R. Minikayev, W. Paszkowicz, J. Crystal Growth. **310**, 284–289 (2008).
[14] L. Armelao, M. Fabrizio, S. Gialanella, F. Zordan, Thin Solid Films. **394**, 90 (2001).
[15] H.H. Mohammad, K.S. Mohammad, Journal of Nanomaterials. (2008).
[16] G. Srinivasan, J. Kumar, Cryst. Res. Technol. **41**(9), 893–896 (2006).
[17] R.C. Brundle, C.A. Evans (Jr.), S. Wilson, Encyclopaedia of Materials Characterization: Surfaces, Interfaces, Thin Films (Materials Characterization Series), Butterworth-Heinemann, Stoneham, (1992), 416-427.
[18] J. Coates, Interpretation of Infrared Spectra, A Practical Approach in Encyclopedia of Analytical Chemistry, R.A. Meyers (Ed.), John Wiley & Sons Ltd, Chichester, 10815–10837 (2000),.
[19] D. Geetha, T. Thilagavathi, Digest Journal of Nanomaterials and Biostructures. **5**(1), 297 (2010).
[20] K. Nakamoto, Infrared and Raman Spectra of Inorganic and Coordination Compounds, Parts A and B. John Wiley & Sons, New York, (1997).
[21] R. Sharma, B.P. Chandra, D.P. Bisen, Chalcogenide Letters. **6**(8),339 (2009).
[22] B.E. Waren, X-ray Diffraction, Addison-Wesley, Reading, MA, (1969).
[23] O.W. Perez-Lopez, A.C. Farias, N.R. Marcilio, J.M.C. Bueno, Materials Research Bulletin. **40,** 2089 (2005).
[24] C. Gümüş, O.M. Ozkendir, H. Kavak, Y. Ufuktepe, Journal of Optoelectronics and Advanced Materials. **8**(1), 299 (2006).
[25] H. Bahadur, A.K. Srivastava, D. Haranath, H. Chander, A. Basu, S.B. Samanta, K.N. Sood, R. Kishore, R.K. Sharma, Rashmi, V. Bhatt, P. Pal, S. Chandra, Indian Journal of Pure & Applied Physics. **45**, 395 (2007) -399.
[26] P. Sagar, M. Kumar, R.M. Mehra, Materials Science-Poland. **23**(3), 685 (2005).
[27] N. Singh, S. Mittal, K.N. Sood, Rashmi, R.K. Gupta, Chalcogenide Letters. **7**(4), 297 (2010).
[28] M.W. Cho, C. Harada, H. Suzuki, T. Minegishi, T. Yao, H. Ko, K. Maeda, I. Nikura, Superlattices and Microstructures. **38**, 349 (2005).
[29] R. Thangavel, V. Sabarinathan, S. Ramasamy, J. Kumar, Materials Letters. **61,** 4090 (2007).
[30] M. Wang, S.H. Hahn, J.S. Kim, J.S. Chung, E.J. Kim, K.K. Koo, J. Crystal Growth. **310**, 1213 (2008).
[31] E. Suvaci, I.O. Özer, Journal of the European Ceramic Society. **25**, 1663 (2005).
[32] B.S. Amma, K. Manzoor, K. Ramakrishna, M. Pattabi, Materials Chemistry and Physics. **112**, 789 (2008).
[33] S. Tanunchai, S. Towta, N. Mangkorntong, P. Mangkorntong, S. Choopun, Chiang Mai J. Sci. **32**(3), 453 (2005).
[34] R.P. Chahal, S. Mahendia, A.K. Tomar, S. Kumar, Chalcogenide Letters. **7**(8), 569 (2010).